Modulation on coherent vortex structures by dispersed solid particles in a three-dimensional mixing layer

Jianren Fan,[1,*] Kun Luo,[1] Youqu Zheng,[2] Hanhui Jin,[1] and Kefa Cen[1]
[1]*Institute for Thermal Power Engineering and CE & EE, Zhejiang University, Hangzhou 310027, China*
[2]*Department of Mechanical Engineering, Zhejiang University of Science and Technology, Hangzhou 310012, China*
(Received 22 April 2002; published 19 September 2003)

Large-scale vortex structures and their effects on the dispersion of particles in turbulent free shear flows are very important in many industrial applications, such as combustion, pollution control, and materials processing. In order to understand large-scale vortex structures and particle dispersion in depth, as well as their interaction effects, a two-way-coupled three-dimensional mixing layer laden with particles at a Stokes number of 5 initially located in the upper half region is studied numerically. A pseudospectral method was used to directly simulate the flow fluid, and the Lagrangian approach was used to trace particles. The concept of computational particles is introduced to vary the mass loading of particles. The momentum coupling effect introduced by a particle approximates to a point force. The simulation results show that coherent structures are still dominant in the mixing layer, but the flow dynamics and particle dispersion are modulated. The length of large-scale vortex structures is shortened and the pairing is delayed. Higher mass loading results in lower energy of the fluid in the phase of Kelvin-Helmholtz rolling up, while in the pairing process of large-scale vortex structures, the energy of the fluid increases as the mass loading increases. Higher mass loading also leads to larger mixed fluid thickness and Reynolds stresses of the flow. In addition, the particle dispersion along the transverse direction differs from that along the spanwise direction, which indicates that the effects of the addition of a particle on the spanwise large-scale vortex structures are different from those on the streamwise large-scale vortex structures.

DOI: 10.1103/PhysRevE.68.036309 PACS number(s): 47.55.Kf, 47.32.Cc

I. INTRODUCTION

Large-scale vortex structures and particle dispersion in turbulent free shear flows are of profound importance in the areas of mixing, combustion, and other related engineering applications. A plane mixing layer is the classical field for the study of turbulence in free shear layers, and has been extensively studied both numerically and experimentally for decades. It is very important to understand the fundamentals of eddy pairing and particle dispersion in the plane mixing layer for many processes such as boiler combustion, particle feed jets, and oil droplet fueled gas combustors.

A comprehensive investigation of the mixing layer generated by a single stream discharging into a quiescent surrounding fluid was made by Liepmann and Laufer, who proved that the flow is self-preserving [1]. The self-preservation shows that the important parameters of the flow are independent of Reynolds number and become similar when rendered dimensionless through division by a single velocity and length scale. Large coherent eddies in a plane turbulent mixing layer were first reported on the basis of flow visualization [2]. From then on, many researchers have focused on the large-scale vortex structures in the mixing layer. Studies of large-scale spanwise vortex structures can be found in [3]. In addition to the primary two-dimensional vortical structure, a well-organized array of streamwise vortices that are superimposed on the spanwise eddies has been observed [4–7]. Although the two-dimensional large vortex structures are quite stable, some experimental results have shown that they are still subject to three-dimensional instabilities. Investigations concerning three-dimensional evolution of a plane mixing layer have been simulated in detail, in which the mechanisms responsible for the growth of three-dimensionality and the onset of transition to turbulence have been described [8]. The development of the complex interactions between small and large vortex structures has also been visualized and characterized by experiment [9].

Experimental investigations of a plane chemically reacting mixing layer ascertained that the coherent streamwise vertical structures were the result of an unstable response to three-dimensional perturbations in upstream conditions and they were always first found on the braids between the spanwise vortices [10]. The transition to three-dimensionality depends on the magnitude and location of the upstream disturbances. Meanwhile, the streamwise vortex tubes undergo nonlinear interactions with the spanwise vortices on the spanwise vortex cores in the three-dimensional development of a plane free shear layer that is subject to small sinusoidal perturbations periodically placed along the span direction [9]. Moreover, the formation of streamwise vortices has been theoretically predicted and numerically simulated [11–15]. The streamwise vorticity emerging in the shear layer always stretches the braids between consecutive spanwise vortices under the positive strain existing in the region and then propagates into their cores.

Many numerical and experimental studies have also been examined the particle dispersion and the associated effects of organized large-scale structures. The Stokes number of particles was introduced to study the particle dispersion; particles with small Stokes number closely follow turbulent

*Corresponding author. Email address: fanjr@mail.hz.zj.cn

flow and particles with large Stokes number are little affected by the fluid flow. However, particles with intermediate Stokes number might be dispersed significantly faster than the fluid motion due to the centrifugal effect created by the organized vortex structures [16]. Particle dispersion in decaying isotropic and homogeneous turbulence has also been simulated using a spectral method and finite-difference schemes [17]. Recently, predictions of the three-dimensional features of particle dispersion in a plane mixing layer have been widely made [18–20]. The results showed that the presence of streamwise vortices leads to additional effects that will modify the dispersion patterns of particles along the spanwise and transverse directions. With the intense three-dimensional vortex stretching and folding, ''mushroom'' shapes of the particle distribution gradually form in the spanwise direction.

The simulations above are all based on one-way coupling, i.e., ignoring the particles' counteractive forces and considering only the effect on particle dispersion of the fluid. This may be correct when the volume fraction of particles is under 10^{-6}. However, in some conditions the local volume fraction of particles may reach 25 times the mean volume fraction of the whole flow region [21]. In this case, the particles can modify the structures of turbulence, and this modification in turn affects particle dispersion.

The particle-turbulence interaction has been extensively investigated. Available experimental data show that the addition of particles may increase or decrease the turbulence kinetic energy of the carrier fluid. Particles with lower Reynolds number cause suppression of the turbulence, while particles with higher Reynolds number cause enhancement of the turbulence due to wake shedding [22]. Larger polystyrene particles cause an increase in the number of wall ejections, the measured values of the turbulence intensities, and Reynolds stresses, while smaller polystyrene particles bring about a decrease in the number of wall ejections, the measured intensities, and Reynolds stresses. In addition, these effects are enhanced as the particle loading increases [23]. All this work by various researchers was brought together and a simple physical model proposed to explain the increase or decrease of turbulent intensity caused by the addition of particles. The ratio of the particle diameter to the length scale of the most energetic eddy is a key parameter. When the ratio is above 0.1 the turbulence intensity is enhanced, while for a ratio below 0.1 it is suppressed [24]. However, particles with low Reynolds number can also increase the turbulence energy in a homogeneous particle-laden turbulence [25]. In forced homogeneous, isotropic, stationary turbulence, the particles increase the turbulent kinetic energy at high wave numbers and decrease it at low wave numbers [26,27]. Recently, the linear stability of a two-way momentum-coupled particle mixing layer was studied by using the Orr-Sommerfeld equation and the results showed that the addition of particles with small Stokes number destabilizes the flow, particles with moderate and large Stokes numbers stabilize the flow, whereas particles with Stokes number of order unity have the most stabilizing effect on the flow [28].

How the particles affect the large-scale vortex structures of the mixing layer have also been examined. The momentum coupling delays the vortex development process without noticeably affecting the mechanisms for vortex growth. The roll-up and pairing process for two-way coupling is similar to that for one-way coupling. But the time and length scales become larger, and vortex structures segregate and even arise out of the forcing from the momentum coupling terms for particles at intermediate Stokes number in the two-dimensional temporal mixing layer [29,30]. The two-way coupled interaction between particles located in the whole fluid field and mixing layer has recently been investigated, and the results showed that particles at intermediate Stokes numbers stabilize the flow, while particles at small Stokes numbers at a particular mass loading tend to destabilize the flow and enhance the mixing [31].

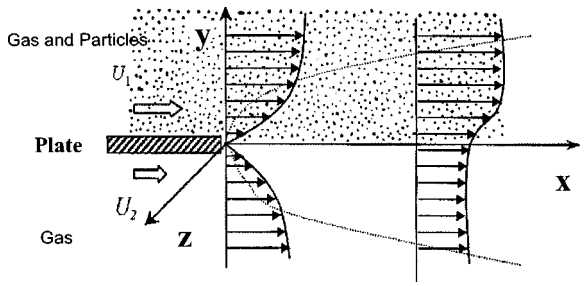

FIG. 1. Sketch of the particle-laden turbulent free shear layer consisting of two parallel streams with different velocities U_1 and U_2 $(U_1 > U_2)$.

The objective of this study is to examine the interaction between particles located in the upper region initially and large-scale vortex structures in a three-dimensional temporal particle-laden mixing layer. We place emphasis on the effects on the large-scale coherent structures by particles with intermediate Stokes numbers and different mass loadings. Some of the turbulence dynamic characteristics and particle dispersion are also included.

Since the early 1970s, direct numerical simulation (DNS) has become an increasingly useful tool to research turbulent flows. In this paper, we will first show the DNS results for the flow field modulation and then give the results for the particle dispersion.

II. NUMERICAL SCHEME

A. Governing equations and initial conditions for flow field

Figure 1 shows a sketch of the particle-laden turbulent free shear layer consisting of two parallel streams with different velocities U_1 and U_2 $(U_1 > U_2)$. If a particle's momentum coupling effect can approximate to a point force, then the nondimensional momentum and continuity equations for an incompressible flow with no body force can be expressed as follows:

$$\frac{\partial \mathbf{U}}{\partial t} = \mathbf{F} - \boldsymbol{\nabla}\Pi + \frac{1}{\mathrm{Re}}\nabla^2\mathbf{U} + \mathbf{F}_p, \tag{1}$$

$$\boldsymbol{\nabla}\cdot\mathbf{U} = 0, \tag{2}$$

where $\mathbf{U}$ is the instantaneous velocity of the fluid, the vorticity $\boldsymbol{\omega}=\nabla\times\mathbf{U}$, $\mathbf{F}=\mathbf{U}\times\boldsymbol{\omega}$, Π is the total pressure, and t is the time. $\mathbf{F}_p$ is the total counterforce caused by all particles in the control volume and can be defined as $\mathbf{F}_p=\Sigma_i^N F_{ip}=\Sigma_i^N \rho_p' f(V-U)/\mathrm{St}$, where ρ_p' is the local bulk density of a particle, N is the total number of particles in the control volume, V is the velocity of the ith particle, and U is the corresponding flow velocity at the position of that particle, which can be obtained by interpolation. St is the Stokes number of the particle defined as $\mathrm{St}=(\rho_p d_p^2/18\mu)/(\theta_0/U_0)$, and f is the modification factor for the Stokes drag coefficient, which is described by $f=1+0.15\,\mathrm{Re}_p^{0.687}$ [33]. Re_p represents the relative Reynolds number for particles, and is defined as $\mathrm{Re}_p=|\mathbf{U}-\mathbf{V}|d_p/\nu$. The flow Reynolds number $\mathrm{Re}=U_0\theta_0/\nu$, in which $U_0=U_1-U_2$ and θ_0, the initial momentum and thickness of the flow, are taken as the velocity and length scale, respectively, and ν is the kinematical viscosity of the fluid. In the present paper, all the simulation parameters are changed to be dimensionless.

The initial conditions for the temporally developing mixing layer are described as follows.

(i) The base flow: a hyperbolic-tangent profile is used to describe the initial mean velocity field, which is given as a function of the transverse direction y: $u_0=0.5U_0\tanh(y)$, where $U_0=(U_1-U_2)$.

(ii) The two-dimensional perturbation: the stream function is derived from the linear Orr-Sommerfeld equations [32], in which the amplitudes were set as $A_1=0.15$ and $A_2=0.08$. Corresponding to the most unstable perturbations, the fundamental wave number α_1 was set to be 0.4446, and the subharmonic unstable wave number α_2 satisfies the condition of resonance $(\alpha_2=\alpha_1/2)$.

(iii) The initial three-dimensional perturbation: the initial streamwise vorticity can be written as $\omega_x=A_3\exp(-y^2/2)\sin(\alpha_3 z)$, in which the amplitude $A_3=0.05$, and α_3 represents the spanwise wave number and is set to be $1.5\alpha_1$ since it has been found that the disturbance with this α_3 is the most unstable [9].

B. Numerical method and procedure

A pseudospectral method was employed to solve the governing equations above. Along the homogeneous directions (x, z), spatial derivatives are expressed by Fourier expansions due to the periodic boundary conditions. The periodicity lengths in the streamwise and spanwise directions are $T_x=2\pi/\alpha_2$ and $T_z=2\pi/\alpha_3$ respectively. In the transverse direction (y), since the perturbation attenuates rapidly along this direction, the solutions in this direction can also be represented by the same expansion by employing mirror image extension. The half-periodicity length in this work is $T_y=30$. The integral area D is defined as $(0,T_x)\times(-T_y/2,T_y/2)\times(0,T_z)$; the number of collocation points in this computational domain is $I\times J\times K=128\times128\times64$.

So all the quantities in Eq. (2) can be expressed by Fourier expansions in the x, y, and z directions as follows:

$$\mathbf{U}(\mathbf{x},t)=\sum_{|k_1|\leqslant I/2}\sum_{|k_2|\leqslant J/2}\sum_{|k_3|\leqslant K/2}\mathbf{u}(\mathbf{k},t)\exp(i\mathbf{k}_\alpha\cdot\mathbf{x}), \quad (3)$$

$$\Pi(\mathbf{x},t)=\sum_{|k_1|\leqslant I/2}\sum_{|k_2|\leqslant J/2}\sum_{|k_3|\leqslant K/2}\pi(\mathbf{k},t)\exp(i\mathbf{k}_\alpha\cdot\mathbf{x}), \quad (4)$$

$$\mathbf{F}(\mathbf{x},t)=\sum_{|k_1|\leqslant I/2}\sum_{|k_2|\leqslant J/2}\sum_{|k_3|\leqslant K/2}\mathbf{f}(\mathbf{k},t)\exp(i\mathbf{k}_\alpha\cdot\mathbf{x}), \quad (5)$$

$$\mathbf{F}_p(\mathbf{x},t)=\sum_{|k_1|\leqslant I/2}\sum_{|k_2|\leqslant J/2}\sum_{|k_3|\leqslant K/2}\mathbf{f}_p(\mathbf{k},t)\exp(i\mathbf{k}_\alpha\cdot\mathbf{x}), \quad (6)$$

in which $\mathbf{u}(\mathbf{k},t)$, $\pi(\mathbf{k},t)$, $\mathbf{f}(\mathbf{k},t)$, and $\mathbf{f}_p(\mathbf{k},t)$ are the Fourier coefficients of velocity $\mathbf{U}(\mathbf{x},t)$, total pressure $\Pi(\mathbf{x},t)$, nonlinearity term $\mathbf{F}(\mathbf{x},t)$, and particle counterforce $\mathbf{F}_p(\mathbf{x},t)$, respectively, $\mathbf{x}=(x,y,z)$, $\mathbf{k}=(k_1,k_2,k_3)$, $\mathbf{k}_\alpha=(2\pi k_1/L_x,2\pi k_2/L_y,2\pi k_3/L_z)$, and $i=\sqrt{-1}$.

By substituting Eqs. (3)–(5) into Eqs. (1) and (2) to give all the Fourier coefficients above, the spatial quantities can be obtained by Fourier reverse transformation. The time advancement of the equations is completed by the two-level explicit Adams-Bashforth scheme for the nonlinearity term $\mathbf{f}(\mathbf{k},t)$ and feedback term $\mathbf{f}_p(\mathbf{k},t)$ as well as the implicit Crank-Nicolson method for the other terms. The computational time step is set to be $\Delta t=0.05$ and $\mathrm{Re}=200$.

C. Particle motion simulation

In the particle dispersion simulation, several assumptions about the particles are made first.

(i) All particles are rigid spheres with identical diameters d_p and densities ρ_p.

(ii) The ratio of the material density for the particles to the material density for the fluid approximates to 2000.

(iii) The particle's gravity is neglected.

(iv) Initially, all the particles have a uniform distribution in the upper section of the flow and retain dynamic equilibrium with the mean flow. This initial particle distribution is the essential difference from the study of Ling *et al.* [31].

(v) We consider the flow as a dilute two-phase flow and the particle-particle interaction is neglected.

With these assumptions, the nondimensional motion equation of a particle can then be expressed as follows:

$$\frac{d\mathbf{V}}{dt}=f/\mathrm{St}(\mathbf{U}-\mathbf{V}) \quad (7)$$

where $\mathbf{V}$ is the velocity of the particle, and $\mathbf{U}$ is the velocity of the fluid at the position of that particle. Then the velocity and position of a particle can be obtained by integrating Eq. (7):

$$\mathbf{V}^{n+1}=\mathbf{U}+\frac{\mathrm{St}}{f}g+\left(\mathbf{V}^n-\mathbf{U}-\frac{\mathrm{St}}{f}g\right)\exp(-f\Delta t/\mathrm{St}), \quad (8)$$

$$\mathbf{X}_p^{n+1}=\mathbf{X}_p^n+\mathbf{U}\Delta t+\frac{\mathrm{St}}{f}g\Delta t+\frac{\mathrm{St}}{f}\left(\mathbf{V}^n-\mathbf{U}-\frac{\mathrm{St}}{f}g\right)\times[1-\exp(-f\Delta t/\mathrm{St})], \tag{9}$$

where the fluid velocity U and f can be treated as constants during the integration over a small enough time step. Since there is only the velocity of the fluid field at every grid point, we use the third Lagrange interpolating polynomial to get the flow velocities at the positions of the particles.

III. SIMULATION RESULTS AND DISCUSSION

A. Flow field modulation

Studies have shown that particles with Stokes number of the order of unity have the largest concentration near the outer edges of the large-scale spanwise vortex structures in the three-dimensional temporal mixing layer [20,34]. So the local particle density should be very large and may cause strong modulation of the fluid. In this work, particles with Stokes number of 5 and different mass loadings are especially considered. The change of the particle mass loading falls back on the concept of computational particles. A computational particle represents a group of particles with the same velocity and position [17]. The number of computational particles in this work is $64\times64\times32$. Four two-way-coupled cases with particle mass loadings of 0.1, 0.3, 0.6, and 1.0 are simulated and compared with one-way coupling. The effect of the research is stressed on the modulations of the large-scale vortex structures, the different energy developments, and the flow dynamics.

1. Modulation of large-scale vortex structures

In order to show clearly the effect on the large-scale vortex structures by particles, we have simulated the gas vorticity field. Three-dimensional contours of the spanwise vorticity at $T=35$ with different mass loadings are shown in Fig. 2. The solid lines represent positive values of the vorticity and the dashed lines represent negative values. From the figure, it can be seen that the size of large-scale spanwise vortex structures becomes smaller and the vortex tubes become rougher with increase of the particle mass loading. When the mass loading equals 0.1, the influence is small, but as the mass loading increases to 0.3 and 0.6, the modulation of vortex structures is obvious and some opposite sign vortex structures can be observed in the area of congregation of particles. The vortex tube structures in the upper half area are destroyed, while they are still obvious in the under half area because there are fewer particles. Although the vorticity is not as smooth as that of the one-way-coupled case, its development is not changed radically by the action of the particles. Similar results can be observed in the three-dimensional contours of streamwise vorticity.

2. Modulation of flow energy

In order to examine how the particles affect the evolution of roll-ups and pairing of the large-scale vortex structures, the development of the energy in the streamwise fundamental and subharmonic Fourier modes is simulated. We define the energy of the streamwise fundamental Fourier mode as $E_{(2,0)}$ and the energy of the streamwise subharmonic Fourier mode as $E_{(1,0)}$. Here,

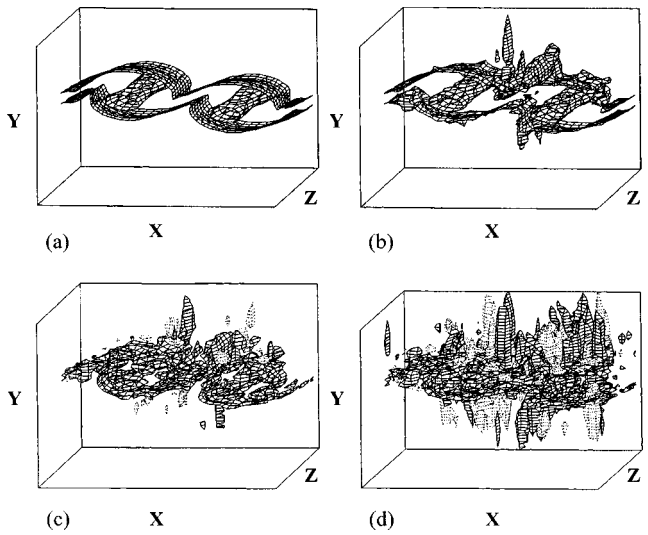

FIG. 2. Three-dimensional contours of spanwise vorticity at nondimensional time $T=35$ for different ratios of particle mass to fluid mass in the unit volume Z_m. (a) One-way coupling (considering only the fluid's effects on particles); (b) $Z_m=0.1$; (c) $Z_m=0.3$; (d) $Z_m=0.6$.

$$E_{(2,0)}=\sum_{k_2} U_{3d}|_{k1=2,k3=0}, \tag{10}$$

$$E_{(1,0)}=\sum_{k_2} U_{3d}|_{k1=1,k3=0}. \tag{11}$$

We also define the energy of the base flow E_0 as

$$E_0=\sum_{k_2} U_{3d}|_{k1=0,k3=0}, \tag{12}$$

where

$$U_{3d}=|u_1(\mathbf{k},t)|^2+|u_2(\mathbf{k},t)|^2+|u_3(\mathbf{k},t)|^2,$$

and $u_1(\mathbf{k},t)$, $u_2(\mathbf{k},t)$, and $u_3(\mathbf{k},t)$ are the Fourier coefficients of the velocities U_1, U_2, and U_3, respectively. $E_{(2,0)}$ and $E_{(1,0)}$ can be nondimensionalized by E_0.

Figure 3 shows the development of $E_{(2,0)}$ for cases with different mass loadings. The energy at fundamental wave number is reduced by the addition of particles and a higher mass loading results in a lower energy of these large-scale vortex structures in the process of the Kelvin-Helmholtz roll-ups. But in the course of vortex pairing, a reverse result is found, which is different from the results of Ling *et al.* [31]. When $T>75$, the addition of particles increases the energy at the fundamental wave number, and the higher mass loading results in higher energy and a longer time to reach the local highest energy value. These changes may be associated with the preferential concentration of the particles. In the first

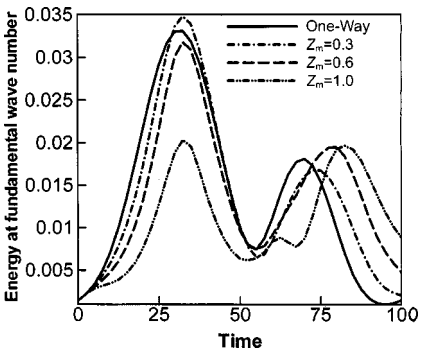

FIG. 3. Development of the energy at streamwise fundamental wave number ($E_{(2,0)}$) with nondimensional time for different ratios of particle mass to fluid mass in the unit volume Z_m.

phase (vortex roll-ups), the particles need to respond to the flow movement and much flow energy has to be consumed. So the flow energy is depressed. But with the development of the random perturbation to the flow field that is introduced by the force coming from the momentum coupling effect of all particles, more energy dissipates and cascades from large- to small-scale turbulence. This is the reason for the enhancement of the energy after the vortex pairing.

The development of the energy in the streamwise subharmonic Fourier mode is similar to the development of energy in the streamwise fundamental Fourier mode. In the process of roll-up, a higher mass loading leads to a lower energy; however, it leads to a higher energy in the pairing process.

It is also found that the addition of particles can enhance the energy of all the Fourier modes with nonzero spanwise wave number, and the enhancement increases with augmentation of the mass loading. This result is well consistent with the corresponding result of Ling *et al.* [31] and the figure is not included.

The total kinetic energy of the flow is shown in Fig. 4. It is obvious that the addition of particles decreases the total kinetic energy compared with one-way coupling, and the kinetic energy is decreased more with increasing mass loading when $T<35$, while the total kinetic energy is enhanced and the larger mass loading results in a higher kinetic energy in the process of vortex pairing. But when $T>75$, the total kinetic energy decays again, and the higher is the mass loading, the faster is the decay.

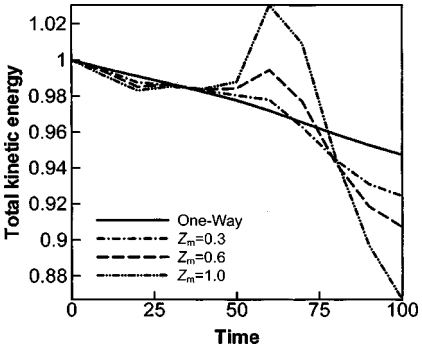

FIG. 4. Development of the total kinetic energy with nondimensional time for different ratios of particle mass to fluid mass in the unit volume Z_m.

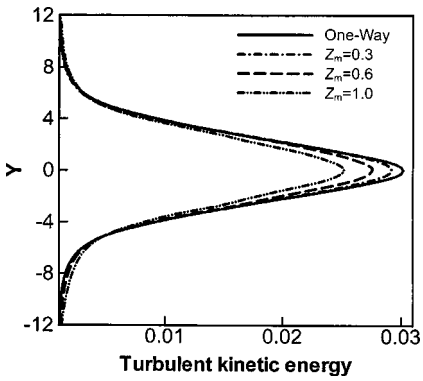

FIG. 5. Distribution of the turbulent kinetic energy along the transverse direction Y at nondimensional time $T=35$ for different ratios of particle mass to fluid mass in the unit volume Z_m.

Figure 5 shows the distribution of the turbulent kinetic energy along the transverse direction when $T=35$. It is clear that in the region of $|Y|>5$ the turbulent kinetic energy for two-way coupling is larger than that for one-way coupling, and the larger mass loading brings larger turbulent kinetic energy, while in the region of $|Y|<5$, the turbulent kinetic energy decays under one-way coupling, and the larger the mass loading, the smaller is the turbulent kinetic energy. In the plane of $Y=0$, the turbulent kinetic energy for each case reaches its maximum value due to the locally maximum fluctuating velocities, while the maximum value decreases as the mass loading increases. This result accords with the corresponding result of Ling *et al.* [31]. It should be pointed out that the kinetic energy distribution is not strictly symmetric because the initial particle distribution is not symmetric. But due to the shorter time of interaction, the general effect on the kinetic energy of the particles is not significant. So the kinetic energy distribution is similar between the upper and lower regions.

The distribution of the turbulent kinetic energy along the transverse direction at the time of 75 is shown in Fig. 6. Higher mass loading results in higher turbulent kinetic energy over all the transverse positions, which is distinct from the conclusion of Ling *et al.* [31] and indicates that the addition of the particles strengthens the turbulent kinetic energy of the fluid in the process of pairing.

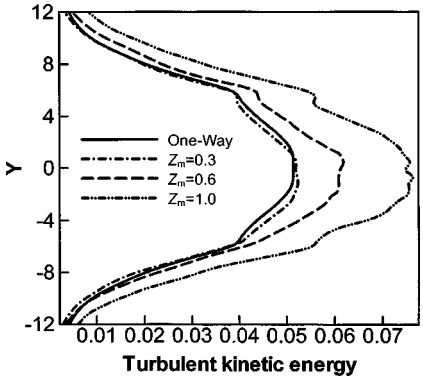

FIG. 6. Distribution of the turbulent kinetic energy along the transverse direction Y at nondimensional time $T=75$ for different ratios of particle mass to fluid mass in the unit volume Z_m.

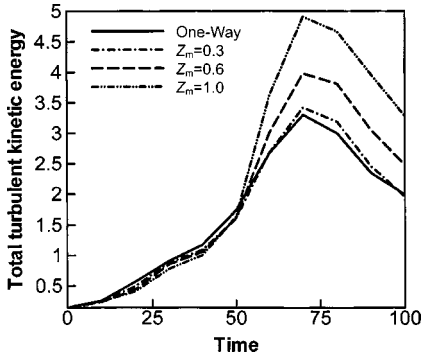

FIG. 7. Development of the total turbulent kinetic energy with nondimensional time for different ratios of particle mass to fluid mass in the unit volume Z_m.

The development of total turbulent kinetic energy with increasing time is also simulated in this paper. The total turbulent kinetic energy T_e is defined as

$$T_e=\frac{1}{2}\left(\frac{1}{T_xT_yT_z}\int_0^{T_x}\int_0^{T_z}\int_{-T_y/2}^{T_y/2}[U_1'^2(x,y,z)+U_2'^2(x,y,z)+U_3'^2(x,y,z)]dx\,dz\,dy\right), \tag{13}$$

where $U_1'(x,y,z)$, $U_2'(x,y,z)$, and $U_3'(x,y,z)$ are the three fluctuating velocities, and can be obtained from

$$U_i'(x,y,z)=U_i(x,y,z)-\overline{U_i}(y), \quad i=1,2,3. \tag{14}$$

Here $U_i(x,y,z)$ are the three velocities, and the term $\overline{U_i}(y)$ is the mean velocity along the transverse direction and can be expressed as

$$\overline{U_i}(y)=\frac{1}{T_xT_z}\int_0^{T_x}\int_0^{T_z}U_i(x,y,z)dx\,dz, \quad i=1,2,3. \tag{15}$$

Figure 7 shows the development of the total turbulent kinetic energy. There exists a turning point on the lines at $T=50$. When $T<50$, the Kelvin-Helmholtz structures are rolling up, the addition of particles depresses the total turbulent kinetic energy, and a larger mass loading causes a lower value of T_e. However, the total turbulent kinetic energy is enhanced by the addition of particles when $T>50$ and reaches its maximum value at the pairing time ($T\approx 75$). Furthermore, the larger the mass loading, the higher is the maximum value. When $T>75$, the total turbulent kinetic energy for each case decreases, but the values for two-way coupling are always higher than that for one-way coupling. The reason is that in the rolling-up process part of the turbulent kinetic energy is dissipated and transferred from fluid to particles; however, in the pairing process part of the turbulent kinetic energy is transferred back to the fluid from the particles.

3. Modulation of fluid thickness

Figure 8 shows the development of the momentum thickness for different cases. The momentum thickness is defined as follows:

$$\theta_m=\int_{-\infty}^{\infty}\{0.25-[U_{1m}(y)]^2\}dy, \tag{16}$$

where $U_{1m}(y)$ is the mean velocity of the transverse profile and can be expressed as

$$U_{1m}(y)=\frac{1}{T_xT_z}\int_0^{T_x}\int_0^{T_z}U_1(x,y,z)dx\,dz. \tag{17}$$

Before spanwise large-scale vortex pairing occurs ($T<60$), the momentum thickness of two-way coupling is smaller than that in one-way coupling, and the higher mass loading leads to a smaller momentum thickness. This agrees well with the conclusion of Ling *et al.* [31]. But in the process of vortex pairing, the momentum thickness of the two-way coupling exceeds that of the one-way coupling, and higher mass loading causes larger momentum thickness. Furthermore, there exists a local maximum value of the momentum thickness for every case. The local maximum value of the momentum thickness corresponds to the pairing time $T=75+$few. A larger mass loading results in a larger local maximum value of momentum thickness and a longer time to reach it. This is distinct from the study of Ling *et al.* [31]. In our simulation, the particles are located only in the upper region initially. The effect on the fluid of the particles first occurs in the upper region and then spreads out to the whole fluid area especially in the pairing process. The interactions between particles and fluid and those between the upper and lower fluid strengthen the disturbance caused by the memory effect of the particles. As a result, in the pairing process the momentum thickness for two-way coupling is enhanced beyond that for one-way coupling and a larger local maximum value is observed when the mass loading is higher.

In order to describe how the particles affect the mixing effect of the fluid, we define the mixed fluid thickness δ_m as

$$\delta_m=\int_{-T_y/2}^{T_y/2}M(t,y)dy, \tag{18}$$

where

$$M(t,y)=\frac{\int_0^{T_x}\int_0^{T_z}H(T-\overline{T})(T_t-T)dx\,dz+\int_0^{T_x}\int_0^{T_z}H(\overline{T}-T)(T-T_b)dx\,dz}{\int_0^{T_x}\int_0^{T_z}H(T-\overline{T})(T_t-\overline{T})dx\,dz+\int_0^{T_x}\int_0^{T_z}H(\overline{T}-T)(\overline{T}-T_b)dx\,dz}. \tag{19}$$

Here $T_t=1$, $T_b=0$, $\overline{T}=0.5$, and

$$H(f)=\begin{cases}1, & f\geqslant 0,\\ 0, & f<0.\end{cases} \tag{20}$$

Figure 9 shows the development of the mixed fluid thickness for all cases. The degree of mixing of the fluid increases with increasing time for different cases. The addition of particles enhances the degree of mixing of the fluid and a larger mass loading results in a higher mixed fluid thickness. This result indicates that the particles can strengthen the mixing degree of the two parallel steams.

4. Modulation of Reynolds stress

In order to study how the particles affect the Reynolds stresses of the flow field, we simulate three terms $u'v'$, $u'w'$, and $v'w'$, which are associated with the Reynolds stresses. Here u',v',w' are the fluctuating velocities in the three directions.

The contours of $u'v'$ in the plane $Z=(1/4)T_z$ at $T=70$ are shown in Fig. 10. The particles increase the value of $u'v'$ in some areas and decrease it in other areas. Although the contour becomes rougher with increase of the mass loading, the distribution of $u'v'$ in the whole region is clearly similar between two-way coupling and one-way coupling. Similar trends can be found in the distributions of $u'w'$ and $v'w'$.

So the distribution of the instantaneous Reynolds stresses of the two-way coupling is also similar to that of the one-way coupling, and the trends of the maximum or the minimum value of $u'v'$, $u'w'$, and $v'w'$ in the whole computational space can reflect the difference of the Reynolds stresses between two- and one-way coupling. In this section, we show the development of the maximum and minimum values of the three terms in space with time and then analyze the effect on the Reynolds stresses by the particles.

Figure 11 shows the development of the maximum and the minimum values of the $u'v'$. It is clear that the addition of particles increases the maximum value of $u'v'$, and a higher mass loading results in a higher maximum value of $u'v'$. Around $T=80$, the maximum value of $u'v'$ reaches its apex for each case, and the apex value for the case of $Z_m=1.0$ is twice that for one-way coupling. But the development of the minimum value of $u'v'$ is opposite, higher mass loading resulting in a lower minimum value of $u'v'$.

The development of the maximum and minimum values of $u'w'$ and $v'w'$ is similar to the development of the maximum and minimum values of $u'v'$; higher mass loading leads to higher maximum values and lower minimum values of $u'w'$ and $v'w'$. These results show that addition of particles can increase the absolute value of the instantaneous Reynolds stresses of the fluid field.

5. Modulation of turbulence intensity

The turbulence intensities are also studied to examine the effects of particles. We define the total turbulence intensity as

$T_i(t)$

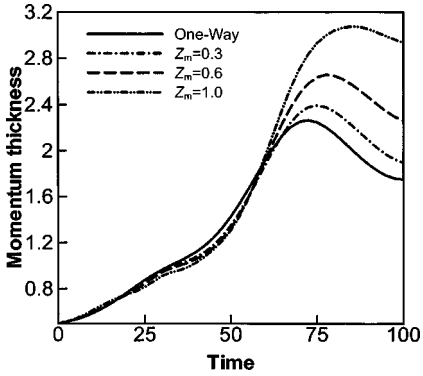

FIG. 8. Development of the momentum thickness with nondimensional time for different ratios of particle mass to fluid mass in the unit volume Z_m.

$$=\int_0^{T_x}\int_0^{T_z}\int_{-T_y/2}^{T_y/2}\sqrt{u'^2(x,y,z)+v'^2(x,y,z)+w'^2(x,y,z)}\times dx\,dz\,dy. \tag{21}$$

The streamwise direction turbulence intensity is defined as

$$T_{xi}(t)=\int_0^{T_x}\int_0^{T_z}\int_{-T_y/2}^{T_y/2}\sqrt{u'^2(x,y,z)}dx\,dz\,dy. \tag{22}$$

The transverse direction turbulence intensity is defined as

$$T_{yi}(t)=\int_0^{T_x}\int_0^{T_z}\int_{-T_y/2}^{T_y/2}\sqrt{v'^2(x,y,z)}dx\,dz\,dy \tag{23}$$

and the spanwise direction turbulence intensity is defined as

$$T_{zi}(t)=\int_0^{T_x}\int_0^{T_z}\int_{-T_y/2}^{T_y/2}\sqrt{w'^2(x,y,z)}dx\,dz\,dy, \tag{24}$$

where $u'(x,y,z)$, $v'(x,y,z)$, and $w'(x,y,z)$ are the fluctuating velocities along the streamwise direction, the transverse direction, and the spanwise direction, respectively. $T_i(t)$, $T_{xi}(t)$, $T_{yi}(t)$, and $T_{zi}(t)$ can be nondimensionalized using their initial values $T_i(0)$, $T_{xi}(0)$, $T_{yi}(0)$, and $T_{zi}(0)$.

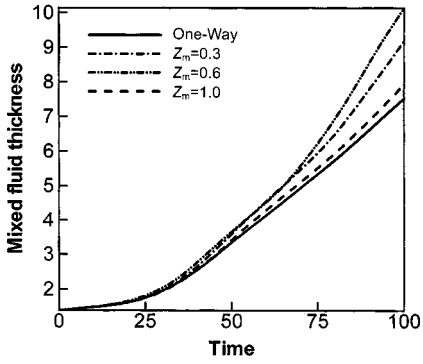

FIG. 9. Development of the mixed fluid thickness with nondimensional time for different ratios of particle mass to fluid mass in the unit volume Z_m.

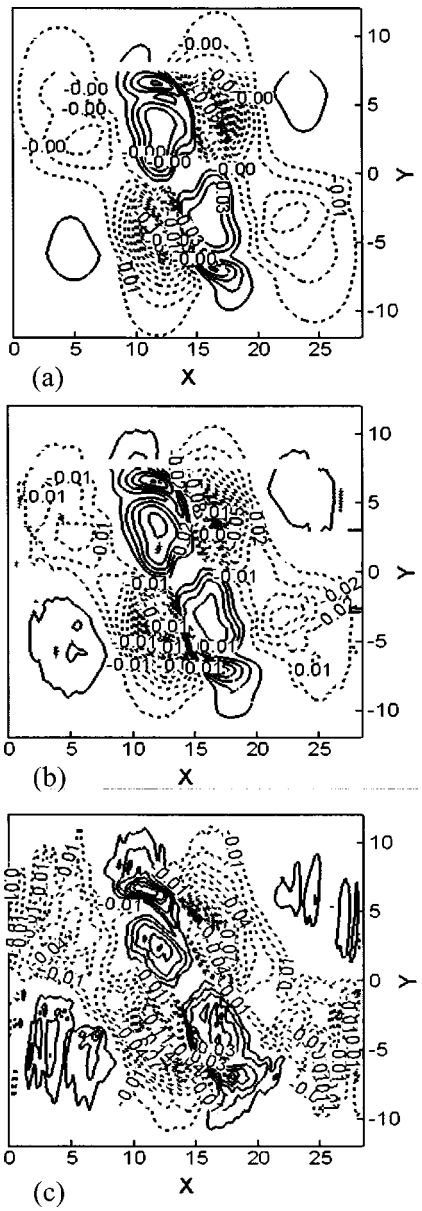

FIG. 10. Contour of Reynolds stress $u'v'$ in the spanwise plane at nondimensional time $T=70$ for different ratios of particle mass to fluid mass in the unit volume Z_m. (a) One-way coupling (considering only the fluid's effects on particles); (b) $Z_m=0.1$; (c) $Z_m=0.3$.

Figure 12 shows the nondimensional results for $T_i(t)/T_i(0)$, $T_{xi}(t)/T_{xi}(0)$, $T_{yi}(t)/T_{yi}(0)$, and $T_{zi}(t)/T_{zi}(0)$. The total turbulence intensity is depressed during the time $T<55$, which corresponds to the course of Kelvin-Helmholtz roll-ups, and the value of $T_i(t)/T_i(0)$ decreases with increasing mass loading. When the vortex structures are going to pair ($T>55$), the total turbulence intensity increases fast and reaches its maximum value around the pairing time ($T\approx 75$). The maximum value is enhanced with enhancement of the mass loading. The development of turbulence intensities along the streamwise and transverse directions is similar to the total turbulence intensity, first a decrease and then an increase.

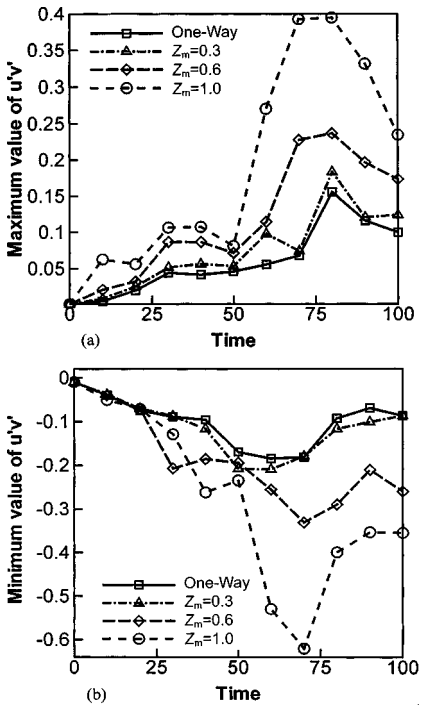

FIG. 11. Development of the maximum and minimum values of Reynolds stress $u'v'$ for different ratios of particle mass to fluid mass in the unit volume Z_m.

The development of the spanwise direction turbulence intensity is different again. In the whole time frame of the simulation, the values of $T_{zi}(t)/T_{zi}(0)$ for the two-way coupling cases are always higher than for one-way coupling, and

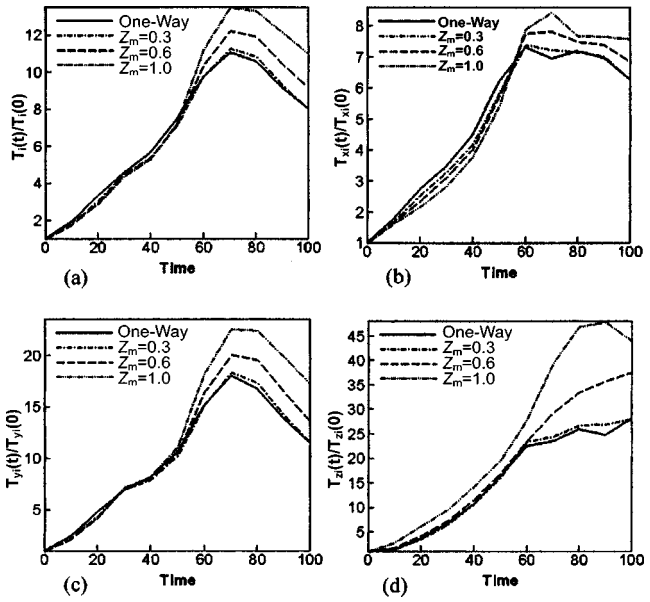

FIG. 12. Development of the total turbulence intensity with nondimensional time for different ratios of particle mass to fluid mass in the unit volume Z_m. (a) Total turbulence intensity T_i; (b) streamwise direction turbulence intensity T_{xi}; (c) transverse direction turbulence intensity T_{yi}; (d) spanwise direction turbulence intensity T_{zi}.

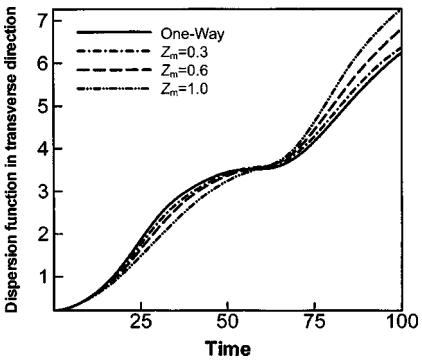

FIG. 13. Particle dispersion along the transverse direction Y for different ratios of particle mass to fluid mass in the unit volume Z_m.

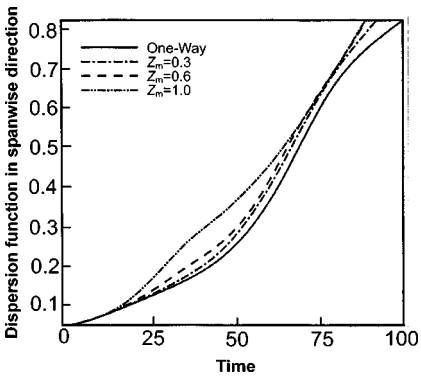

FIG. 14. Particle dispersion along the spanwise direction Z for different ratios of particle mass to fluid mass in the unit volume Z_m.

a larger mass loading results in a smaller spanwise direction turbulence intensity. This indicates that the addition of particles increases the fluctuation level of the fluid along the spanwise direction.

B. Particle dispersion modulation

From a simulation of the flow field, we can see that in the two-way-coupled cases, the particles affect the development of the energy, the vortex structures, and the fluid dynamics in the mixing layer. It is clear that modulation of the fluid field should modulate the particle dispersion in turn. Particle dispersion with Stokes number of 5 and different mass loadings was also numerically simulated in this paper.

To study the particle dispersion level due to the large-scale spanwise structures quantitatively, the dispersion function in the transverse (Y) direction for particles distributed on the $Y=0$ plane is evaluated, as obtained from

$$D_y(t)=\left(\sum_{i=1}^{n_y}[Y_i(t)-Y_m(t)]^2/n_y\right)^{1/2}, \tag{25}$$

where n_y is the total number of particles distributed on the $Y=0$ plane, $Y_i(t)$ is the particle displacement in the transverse direction at time t, and $Y_m(t)$ is the mean value. Figure 13 shows the dispersion function of particles for different cases. There exists a turning point in the plot at $T=75-$few, approximately at the pairing time for spanwise large-scale vortex structures. Before the turning point, the particle dispersion along the transverse direction is depressed, and the value of $D_y(t)$ decreases with increasing mass loading, while after the turning point, the particle dispersion increases, and larger mass loading leads to a larger increase of the particle dispersion. The results also exhibit that the spanwise large-scale vortex structure is depressed by particles in the process of roll-up and then is enhanced in the process of pairing, which is distinct from the corresponding result of Ling *et al.* [31].

The dispersion function in the spanwise direction was also introduced to study the particle dispersion levels quantitatively on the $Z=T_z/4$ plane. The dispersion function is obtained from

$$D_z(t)=\left(\sum_{i=1}^{n_z}[Z_i(t)-Z_m(t)]^2/n_z\right)^{1/2}, \tag{26}$$

where n_z is the total number of particles distributed on the $Z=T_z/4$ plane, $Z_i(t)$ is the particle displacement in the spanwise direction at time t, and $Z_m(t)$ is the mean value.

Figure 14 shows the dispersion function in the spanwise direction for each case. It is apparent that the dispersion for each case increases with time, and higher mass loading results in larger dispersion along the spanwise direction due to the two-way momentum coupling effects. When $T=75+$few, the dispersion values for all cases are comparable, which shows that the development of the streamwise large-scale vortex structure is depressed temporarily at the pairing time of the spanwise large-scale vortex structure. The result indicates that the turbulence along the spanwise direction is enhanced by the addition of particles, which is caused by the development of random perturbation along the spanwise direction introduced by all particles.

IV. CONCLUSIONS

Direct numerical simulation results demonstrate that the presence of particles at a Stokes number of 5 modulates the large-scale vortex structures and the pattern of particle dispersion in a three-dimensional particle-laden mixing layer. Compared with the one-way coupling case, the large-scale vortex structures become shorter, thinner, and rougher in the case of two-way coupling. The addition of particles also increases the energy of all the Fourier mode with nonzero spanwise wave number of the fluid, and this trend is strengthened as the particle mass loading increases. But the developments of the turbulent kinetic energy are not uniform. In the process of Kelvin-Helmholtz rolling up, the particles decrease the turbulent kinetic energy and larger mass loading leads to lower turbulent kinetic energy, while in the process of vortex structure pairing, the particles increase the turbulent kinetic energy and larger mass loading leads to larger turbulent kinetic energy. Similar effects are observed in the development of the energy at fundamental and subharmonic wave numbers, the development of the momentum thickness, and the development of the total turbulence intensity. The Reynolds stresses and the mixed fluid thickness of

the flow are enhanced by the particles, and larger enhancements are found with increasing mass loading. At the same time, the particle dispersion pattern is modulated. The dispersion of particles along the transverse direction differs from that along the spanwise direction. The particle dispersion along the transverse direction is not uniform. In the first phase, the particle dispersion is depressed in each of the two-way coupled cases compared with the one-way coupled case, and larger mass loading results in lower particle dispersion, but after the vortex pairing, the particle dispersion increases and larger mass loading results in larger particle dispersion. This change is associated with the development of spanwise large-scale vortex structures. The trend of the particle dispersion along the spanwise direction is uniform. In the whole time frame of the simulation, the dispersion of particles increases with time and higher mass loading leads to higher particle dispersion.

ACKNOWLEDGMENTS

The authors gratefully acknowledge the support of this research by the Special Funds for Major State Basic Research Projects of the People's Republic of China (Grant No. G19990222-05) and the National Natural Science Foundations of China (Grants No. 50236030 and No. 50076038).

[1] H. W. Liegmann and J. Laufer, NACA Technical Note No. 1257, 1947 (unpublished).
[2] G. L. Brows and A. Roshko, J. Fluid Mech. **64**, 775 (1974).
[3] C. M. Ho and P. Huerre, Annu. Rev. Fluid Mech. **16**, 365 (1984).
[4] J. H. Konard, Technical Report No. CIT-9-PU, 1976 (unpublished).
[5] R. E. Breidenthal, J. Fluid Mech. **97**, 771 (1981).
[6] J. Jimenez, J. Fluid Mech. **123**, 319 (1983).
[7] L. P. Bernal and A. Roshko, J. Fluid Mech. **170**, 499 (1986).
[8] R. D. Moser and M. M. Rogers, J. Fluid Mech. **247**, 275 (1993).
[9] J. C. Lasheras and H. Choi, J. Fluid Mech. **189**, 53 (1988).
[10] J. C. Lasheras, J. S. Cho, and T. Maxworthy, J. Fluid Mech. **172**, 231 (1986).
[11] G. M. Corcos and S. L. Lin, J. Fluid Mech. **139**, 67 (1984).
[12] S. L. Lin and G. M. Corcos, J. Fluid Mech. **141**, 139 (1984).
[13] R. T. Pierrehumbert and S. E. Widnall, J. Fluid Mech. **114**, 59 (1982).
[14] R. W. Metcalfe, S. A. Orszag, M. E. Brachet, S. Menon, and J. J. Rilley, J. Fluid Mech. **184**, 207 (1987).
[15] W. T. Ashurst and E. Meiburg, J. Fluid Mech. **189**, 87 (1988).
[16] C. T. Crowe, R. A. Gore, and T. R. Troutt, Part. Sci. Technol. **3**, 149 (1985).
[17] S. E. Elghohashi, Appl. Sci. Res. **52**, 309 (1994).
[18] B. Marcu and E. Meiburg, Phys. Fluids **8**, 2266 (1996).
[19] X. L. Tong and L. P. Wang (unpublished).
[20] W. Ling, J. N. Chung, T. R. Troutt, and C. T. Crowe, J. Fluid Mech. **358**, 61 (1998).
[21] K. D. Squires and J. K. Eaton, Phys. Fluids A **3**, 1169 (1991).
[22] G. Hetsroni, Int. J. Multiphase Flow **15**, 735 (1989).
[23] M. Rashidi, G. Hetsroni, and S. Banerjee, Int. J. Multiphase Flow **16**, 935 (1990).
[24] R. A. Gore and C. T. Crowe, Int. J. Multiphase Flow **15**, 279 (1989).
[25] S. Elghobashi and G. C. Truesdell, Phys. Fluids A **5**, 1790 (1993).
[26] J. K. Eaton and J. R. Fessler, Int. J. Multiphase Flow **20**, 169 (1994).
[27] M. Boivin, O. Simonin, and K. D. Squires, J. Fluid Mech. **375**, 235 (1998).
[28] X. L. Tong and L. P. Wang (unpublished).
[29] L. Tang, C. T. Crowe, J. N. Chung, and T. R. Troutt (unpublished).
[30] X. L. Tong and L. P. Wang (unpublished).
[31] W. Ling, J. N. Chung, and C. T. Crowe, Proc. R. Soc. London, Ser. A **456**, 2931 (2000).
[32] A. Michalke, J. Fluid Mech. **19**, 543 (1964).
[33] R. Clift, J. R. Grace, and M. E. Weber, *Bubbles, Drops, and Particles* (Academic, New York, 1978).
[34] J. R. Fan, Y. Q. Zheng, J. Yao, and K. F. Cen, Proc. R. Soc. London, Ser. A **457**, 2151 (2001).